THE JOURNAL OF PHYSICAL CHEMISTRY C

Article

pubs.acs.org/JPCC

EXAFS Characterization of PtNi Bimetallic Catalyst Applied to Glycerol Liquid-Phase Conversion

María L. Barbelli,[‡] Martín D. Mizrahi,[§] Francisco Pompeo,[†,‡] Gerardo F. Santori,[†,‡] Nora N. Nichio,*[,†,‡] and Jose M. Ramallo-Lopez[§]

[†]Facultad de Ingeniería, PIDCAT, Universidad Nacional de La Plata, 1 esq 47, 1900 La Plata, Argentina

[‡]CINDECA, Facultad de Ciencias Exactas, Universidad Nacional de La Plata, CCT La Plata-CONICET, 47 no. 257, 1900 La Plata, Argentina

[§]INIFTA, Facultad de Ciencias Exactas, Universidad Nacional de La Plata, CCT La Plata-CONICET, Diagonal 113 y 64, 1900 La Plata, Argentina

Supporting Information

ABSTRACT: The aim of this work is to evaluate the catalytic properties (activity, selectivity, and stability) of PtNi catalysts supported on Ce−Zr−α-Al_2O_3 (CZA) in the liquid-phase conversion of glycerol and to relate them to the results of the EXAFS characterization. The PtNi/CZA catalyst presents the highest global activity and promotes the formation of liquid oxygenated hydrocarbons, mainly acetol and 1,2-propylene glycol, which are formed from glycerol hydrogenolysis. By means of EXAFS studies, it was determined that three phases are present: a $PtNi_3$ nanoalloy, unalloyed metallic Pt with high dispersion, and unalloyed metallic Ni. The highest activity of the PtNi/CZA could be assigned to the presence of the $PtNi_3$ alloy, which results in a more active phase than the Pt and Ni sites separately. The PtNi/CZA is the more stable, and the EXAFS results show that this behavior would be associated with the presence of the $PtNi_3$ alloy nanoparticles on the surface of the Ni particles with low mobility.

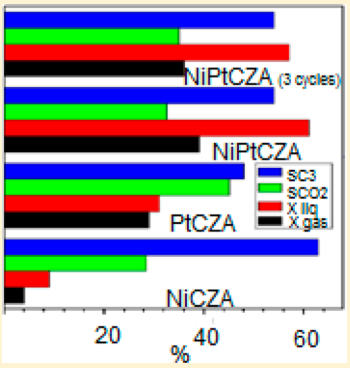

1. INTRODUCTION

In the past few years, the liquid-phase reactions of alcohols coming from biomass like methanol, ethylene glycol, glycerol, sorbitol, etc., have been reported.[1−16] Dumesic and co-workers[1−6] developed the aqueous phase reforming (APR) process to produce hydrogen. This process presents important advantages when compared to the steam reforming: it is highlighted that the vaporization of the mixture is not necessary, reducing the energetic requirement. Also, the decomposition reactions that take place at high temperatures are minimized. H_2 with low CO content is obtained because the water gas shift reaction (WGS) is favored in the APR conditions.[1−6,11,12]

To obtain hydrogen from APR of polyols, an effective catalyst must be active for the C−C bond cleavage, and it must promote the WGS reaction. To obtain liquid oxygenated products the catalyst has to be active in the C−O bond cleavage.

Catalytic systems based on metals of group VIII are cited in bibliography for APR of alcohols.[1−16] Wen and co-workers have reported the decreasing order in the yield to H_2 for APR of glycerol: Pt > Cu > Ni > Co.[8] Different bimetallic systems have also been studied. Huber and co-workers studied the APR of ethylene glycol and found that the systems of PtNi, PtCo, PtFe, and PdFe were more active than the monometallic Pt and Pd catalysts.[5] The modification of a Ni Raney catalyst with Sn increased the yield to H_2 due to a decrease in C−O bond cleavage reactions and inhibition of the methanation reaction.[11,12] King and co-workers studied Pt−Re/C catalysts and suggested that different species coexist in the active phase: Pt−Re alloy and ReO_x species. Pt−Re alloy leads to an increased rate of dehydrogenation and decarbonylation, while ReO_x (acidic) species promote dehydration pathways leading to liquid products (propylene glycol, acids, and alcohols) and alkanes.[13] Additionally, Zhang and co-workers found that with Pt−Re/C catalysts the oxidation of Pt−Re in hydrothermal reaction conditions generates surface acidity, which drastically affects the reaction pathways, and favors C−O over C−C cleavage, which results in higher selectivity to liquid products and alkanes at the expense of hydrogen selectivity.[14]

Iriondo and co-workers studied bimetallic PtNi catalysts supported on γ-Al_2O_3 and La_2O_3−γ-Al_2O_3 in the APR of glycerol. The presence of La_2O_3 improved the catalytic behavior toward lighter gaseous products. The high activity of the PtNi catalysts can be associated with the formation of metal Pt−Ni alloy and the spillover phenomenon.[15] Doukkali and co-workers studied the APR of glycerol with Pt and Ni−γ-Al_2O_3 catalysts. These catalysts prepared by the sol−gel method are intrinsically more active than their equivalent impregnated catalysts. Their higher activities can be explained due to better

Received: December 20, 2013
Revised: September 17, 2014
Published: September 18, 2014

catalytic properties achieved by the sol−gel method in terms of surface area, porosity, finer size of Pt and Ni particles, and synergistic effect between these two elements.[16]

Ravenelle and co-workers studied the structural changes of γ-Al_2O_3, Ni/γ-Al_2O_3, and Pt/γ-Al_2O_3 under APR conditions. It is demonstrated that γ-Al_2O_3 is converted into a hydrated Boehmite (AlOOH) phase with significantly decreased acidity, surface area, and increased sintering of the metal particles.[17]

α-Al_2O_3 is an adequate support due to its high stability, availability, and low cost, although as disadvantages it presents limited surface area and reactivity. These disadvantages in the support lead to catalysts of low metallic dispersion with weak metal−support interaction. According to results obtained in previous work, the addition of small amounts of CeO_2 (4 wt %) and ZrO_2 (1 wt %) to α-Al_2O_3 leads to $Ce_{0.8}Zr_{0.2}O_2$ composite, thus conferring higher reactivity to the surface due to the presence of basic nature sites.[18]

The aim of this work is to evaluate the effect of the addition of Pt to a Ni catalyst supported on α-Al_2O_3 modified with CeO_2 and ZrO_2 oxides in the APR of glycerol. In addition, a detailed structural characterization performed by extended X-ray absorption fine structure (EXAFS) spectroscopy of fresh and used catalyst was carried out to correlate the structure of the catalysts with their catalytic performance and stability after different reaction cycles.

2. EXPERIMENTAL SECTION

2.1. Catalyst Preparation. Commercial α-Al_2O_3 Rhone Poulenc (Spheralite 512; surface area around 10 $m^2\ g^{-1}$) was used as base support. Modified support was prepared by incipient wetness impregnation of α-Al_2O_3 with $ZrO(NO_3)_2 \cdot H_2O$ (Aldrich) and $Ce(NO_3)_3 \cdot 6H_2O$ (Alpha) aqueous solutions. The modified support with 1 wt % of ZrO_2 and 4 wt % of CeO_2 is designated as CZA.[18] The CZA support was dried at 120 °C for 12 h and calcined in air for 4 h at 600 °C. The Pt/CZA catalyst was prepared at room temperature by impregnation with H_2PtCl_6 to reach a final metallic content of 1 wt %. After being dried at 120 °C for 12 h, the sample was calcined in air flow at 500 °C for 2 h. The Ni/CZA catalyst was prepared at room temperature by impregnation with $Ni(NO_3)_2 \cdot 6H_2O$ (Aldrich) aqueous solution to reach a final metallic content of 5 wt %. After being dried at 120 °C for 12 h, the sample was calcined in air flow at 750 °C for 2 h.

The PtNi/CZA bimetallic catalyst was prepared at room temperature by impregnation of Ni/CZA with H_2PtCl_6 to reach a final metallic content of 1 wt % Pt. After being dried at 120 °C for 12 h, the sample was calcined in air flow at 500 °C for 2 h.

2.2. Catalyst Characterization. The Pt and Ni contents were determined by atomic absorption spectrometry (AAS). The calibration curve method was used, with standards prepared in the laboratory. The equipment utilized was an IL model 457 spectrophotometer, with single channel and double beam. The light sources were hollow monocathode lamps.

Transmission electron microscopy (TEM) images were taken by means of a TEM JEOL 100 C instrument, operated at 200 kV. A graphite pattern was used for calibration. In this analysis, a suspension in 2-propanol was prepared by stirring the solid sample with ultrasound for 10 min. A few drops of the resulting suspension were deposited on a TEM Cu grid (Lacey carbon film 300 mesh, electron microscopy science) and subsequently dried and evacuated before the analysis.

XRD patterns were recorded on a powder diffractometer Philips 3020, using Cu Kα radiation (λ = 1.5418 Å, intensity = 40 mA, and voltage = 35 kV). The patterns were recorded in the range of 2θ = 20°−70°. To determine the structural parameters and microstructure of the identified crystalline phases, the XRD patterns were analyzed with the program FULLPROF. The average crystallite size D was estimated using the Scherrer relation where θ is the reflection angle and B is the peak broadening corrected by the instrumental line broadening (0.08°):

$$D = \frac{0.94\lambda}{B \cos \theta} \quad (1)$$

The XPS analysis was carried out in a multitechnique system (Specs), equipped with a dual Mg/Al X-ray source and a hemispherical PHOIBOS 150 analyzer operating in the fixed analyzer transmission (FAT) mode. The spectra were obtained with a pass energy of 30 eV and an Al Kα anode operated at 200 W. The pressure during the measurement was less than 2×10^{-8} mbar. The samples were subjected to a reduction during 10 min at 400 °C in H_2 5%/Ar flux in the pretreatment chamber of the equipment.

EXAFS experiments were measured at the XAFS2 beamline at the LNLS (Laboratorio Nacional de Luz Sincrotron), Campinas, Brazil. EXAFS spectra of the Pt L_3 (11564 eV) and Ni K (8333 eV) edges were recorded at room temperature using a Si (111) single channel-cut crystal monochromator in transmission mode and with three ion chambers as detectors. The third one was used to measure the corresponding metallic reference simultaneously with the sample. The samples were reduced at the desired temperature in a reactor connected to the XAS cells. The powdered samples were transferred under Ar to the XAS cells, which were then sealed to avoid contact with air and were measured in that condition.

The EXAFS data were extracted from the measured absorption spectra by standard methods using the ATHENA software, which is part of the IFFEFIT package.[19] The Fourier transformation was calculated using the Hanning filtering function. EXAFS modeling was carried out using the ARTEMIS program (IFFEFIT package).[19] Structural parameters (coordination numbers and bond lengths and their mean squared disorders) were obtained by a nonlinear least-squares fit of the theoretical EXAFS signal to the data in R space by Fourier transforming both the theory and the data. Theoretical scattering path amplitudes and phase shifts for all paths used in the fits were calculated using the FEFF6 code.[20] The k-range was set from 2−14 $Å^{-1}$, and the Fourier transform was fitted in different regions depending on the sample and the edge. The passive reduction factor S_0^2 was restrained to values of 0.93 and 0.79 for Pt L_3 and Ni K-edges analysis, respectively. These values were obtained from fitting of metallic Pt and Ni foils standards by constraining the coordination number in these compounds of known crystal structure.

2.3. Catalytic Tests. The APR experiments were carried out in a high pressure reactor BR-100 system, from Berghof Instruments, with a volume of 100 mL, operated in batch mode. The magnetic stirring was set at 900 rpm. The reactive mixture, 12 cm^3, was an aqueous solution of 10 wt % glycerol. In a typical experiment, the Pt/CZA and PtNi/CZA catalyst were reduced ex situ at 500 °C for 2 h in H_2 flow (30 $cm^3\ min^{-1}$) using a heating rate of 10 °C min^{-1}, while the Ni/CZA catalyst was reduced ex situ at 750 °C for 2 h at the same conditions, because the TPR profiles (not shown) exhibited high

dx.doi.org/10.1021/jp412512x | J. Phys. Chem. C 2014, 118, 23645−23653

temperatures of reduction (<800 °C) for this sample. The samples after this pretreatment will be described from then on as "fresh catalysts". The catalyst then was introduced in the reaction media under H_2 flow at room temperature. Subsequently, the reactor was purged with N_2 (Air Liquide, 99.99%) and heated to reaction temperature. The catalytic tests were performed at 200 and 250 °C and a pressure of 44 bar.

The main reactions involved in the APR are represented in eqs 2−4:

$$C_3H_8O_3 \leftrightarrow 3CO + 4H_2 \quad \text{(GLY decomposition)} \tag{2}$$

$$CO + H_2O \leftrightarrow CO_2 + H_2 \quad \text{(water−gas shift reaction)} \tag{3}$$

$$C_3H_8O_3 + 3H_2O \leftrightarrow 3CO_2 + 7H_2 \quad \text{(reforming reaction)} \tag{4}$$

The catalytic activity is expressed as the conversion to gaseous products (X^G), the conversion to liquid products (X^L), and the total conversion (X^T), defined as

$$X^G = \frac{\text{C atoms in gas products}}{\text{C initial atoms of glycerol}} \times 100 \tag{5}$$

$$X^T = \frac{N^o - N^f}{N^o} \times 100 \tag{6}$$

$$X^L = X^T - X^G \tag{7}$$

where

N^o = initial moles of glycerol

N^f = final moles of glycerol

The selectivity to carbon products (SCO_2, SCO, SCH_4, S_LC_1, S_LC_2, and S_LC_3) and selectivity to H_2 (SH_2) were defined as

$$SC_n\% = \frac{(\text{mole of the product}) \times (\text{number of carbon atoms in the product})}{\text{mole of glycerol consumed} \times 3} \times 100 \tag{8}$$

$$SH_2\% = \frac{\text{molecules of } H_2 \text{ produced}}{\text{C atoms in gas products}} \times \frac{1}{R} \times 100 \tag{9}$$

where R is the H_2/CO_2 reforming ratio of 7/3 for glycerol.

Three reaction cycles were carried out to evaluate the catalytic stability. Each cycle includes the reduction of the catalyst during 2 h in pure H_2 flow (conditions as mentioned above), the reaction during 2 h at 250 °C, the regeneration in air flow at 500 °C during 2 h, and the reduction in H_2 flow at 500 °C during 2 h.

2.4. Analysis of Products. The analysis of gaseous products was performed with a gas chromatograph Shimadzu GC-8A equipped with a column of 10 m and 1/8" HayeSep DB 110-120 and GC/TCD detector. The liquid products were analyzed by gas chromatography with GC/FID and mass spectrometry CG/MS detector (Shimadzu GCMS-QP5050A) with a 50 m (0.2 mm and 0.5 μm) HP-PONA capillary column. The accuracy of the measured values was within 5%, and the experiments could be reproduced with a relative error of 10%.

3. RESULTS AND DISCUSSION

The support of the catalysts is α-Al_2O_3 (Rhone Poulenc) modified by 1 wt % of ZrO_2 and 4 wt % of CeO_2 (CZA) with a BET area of 8 m^2 g^{-1}. The determination of the acid−base properties by the isopropanol decomposition reaction indicates that CZA is a support with more basic characteristics than the commercial alumina.[18]

Figure 1 shows the XRD diffractograms of Ni/CZA and PtNi/CZA reduced catalysts. The main peak at 2θ = 28.68° is due to the cubic phase of a solid solution of $Ce_{0.8}Zr_{0.2}O_2$.[18] For the Ni/CZA catalysts, the principal peaks of metallic Ni are observed (2θ = 44.5° and 51.7°), with a lattice parameter a = 3.5253 Å. The average crystallite size estimated using the Scherrer relation is 17.7 nm.

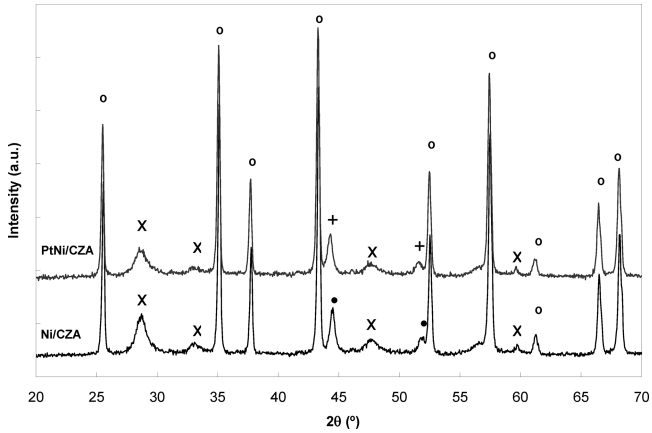

Figure 1. XRD patterns of reduced Ni/CZA and PtNi/CZA catalysts: (○) Al_2O_3, (×) $Ce_{0.8}Zr_{0.2}O_2$, (●) Ni, (+) PtNi.

For the monometallic Pt/CZA catalysts (not shown), the diffraction signal was very weak and broad. This observation suggested that the Pt^0 presented particle size is too small to be detected by this technique.[15]

For the PtNi/CZA catalyst, no signals corresponding to a Pt phase were observed. The Ni lattice parameter obtained was a = 3.5361 Å, which shows a small shift with respect to that of the Ni/ZCA catalysts (a = 3.5253 Å). According to the literature, this observation suggests some Pt−Ni alloy formation.[15,21] For this reason, we use a more specific technique like EXAFS to determine if an alloy of Ni and Pt is present in the bimetallic catalyst.

In a previous work, we determined that Pt catalysts prepared by incipient wetness impregnation on α-Al_2O_3 (Rhone Poulenc) achieve higher metallic dispersion than Ni catalysts, with a particle size of 4 and 18 nm, respectively.[22] TEM results of the modified alumina with Ce and Zr (CZA) show the presence of composite $Ce_{0.8}Zr_{0.2}O_2$ particles with sizes between 8 and 20 nm (Figure 2a). Although it is not possible to clearly distinguish between Ni and support particles in the monometallic sample Ni/CZA (Figure 2b), a bigger number of particles in the range 16−28 nm are found. This is in agreement with XRD estimation of the size of Ni crystallites of 17.7 nm. In the Pt/CZA and PtNi/CZA catalysts (Figure 2c,d), a great number of small particles with sizes between 1 and 2 nm are observed. TEM photographs and the histograms of particle size distribution are included in the Supporting Information.

In Table 1 are shown the results of the APR of glycerol. The gaseous products were mainly H_2 and CO_2. The selectivity to CO_2 (denoted SCO_2) is representative of the selectivity to the reforming reaction (reaction 4). The low CO content, which is close to 1000 ppm in gaseous products, would be indicating that the CO can be quickly converted to CO_2 through the WGS reaction (reaction 3). In Table 1 it is also indicated the

dx.doi.org/10.1021/jp412512x | J. Phys. Chem. C 2014, 118, 23645−23653

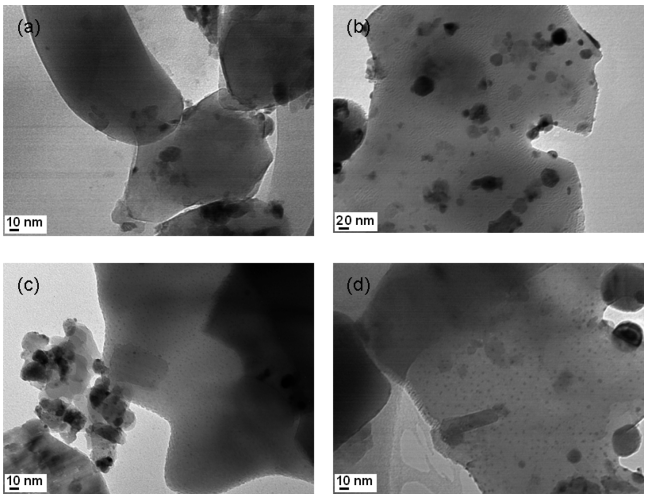

Figure 2. TEM micrographs of (a) CZA, (b) Ni/CZA, (c) Pt/CZA, and (d) PtNi/CZA.

selectivity to liquid products grouped by the number of carbon atoms: S_LC_1 (methanol), S_LC_2 (ethanol and ethylene glycol), and S_LC_3 (acetone, 1-propanol, acetol, propylene glycol). The overall mass balances were always between 96.8% and 99.8%, suggesting negligible conversion of glycerol into unidentified liquid products. The initial TOF values are included in the Supporting Information.

It can be seen in Table 1 that Ni/CZA has very low glycerol conversion (X^T = 17%) as compared to Pt/CZA (X^T = 60%) and PtNi/CZA (X^T = 100%) catalysts. The Pt/CZA catalyst has the highest selectivity to reforming (SCO_2 = 45%). The small particle size and high metallic dispersion of the Pt favor the C−C bond cleavage reactions to produce gases, in accordance with Lercher and co-workers.[23]

The bimetallic catalyst PtNi/CZA has the highest glycerol conversion to liquid products (X^L = 61%) and has lower selectivity to reforming (SCO_2 = 35.2%) than Pt/CZA.

These results agree with those reported by Iriondo and co-workers[15] and Doukkali and co-workers.[16] These authors studied the APR of glycerol (at 240 °C and 40 bar pressure) and found higher conversion of glycerol and higher selectivity to oxygenated hydrocarbons (mainly propylene glycol) with PtNi/alumina catalysts,[15] which was explained by a synergistic effect between both metals and the low metallic dispersion of the catalyst (16−20 nm). In the work of Doukkali and co-workers carried out in a flow reactor, it is reported that the Pt catalysts promoted gas production with higher H_2 selectivity, the Ni catalysts were more selective to alkanes formation, and PtNi catalysts presented an intermediate behavior: moderate H_2 and alkanes selectivity, due to the cooperative effect between both metals.[16]

Table 1 shows the results obtained at the same pressure but at a temperature of 200 °C. The decrease in the level of conversion and a higher selectivity S_LC_3 for the bimetallic catalyst is observed. In Figure 3 are shown the liquid products

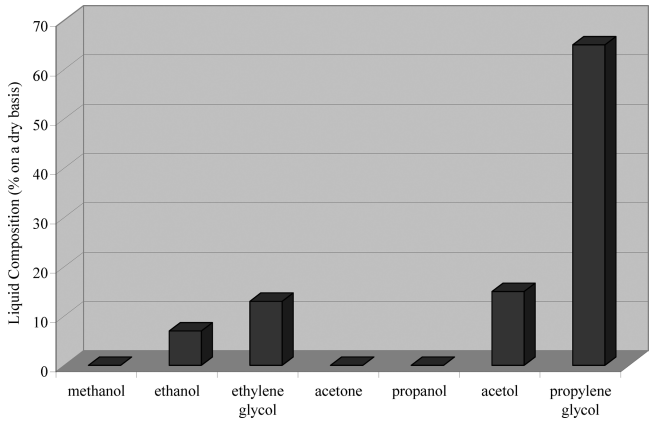

Figure 3. Products identified for PtNi/CZA. Reaction condition: 10 wt % glycerol, T = 200 °C, P = 44 bar, mass of catalysts = 0.5 g, reaction time = 2 h.

identified for PtNi/CZA are shown. This results indicates that the bimetallic catalyst promotes the formation of liquid oxygenated hydrocarbons, mainly acetol and 1,2-propylene glycol, which are formed from glycerol hydrogenolysis. This indicates that the C−O bond cleavage reactions are favored, which might be related to the formation of a new active phase, an aspect that will be investigated by EXAFS.

Because of the severe hydrothermal conditions of this reaction, the stability of the catalysts was evaluated. Figure 4 shows the changes in conversion and selectivity along the three cycles. The results of Pt/CZA indicate that in the second and third cycles, the conversion to liquids products X^L increases considerably due to increases of C−O bond cleavage reactions. In previous work,[24] we determined that with increasing particle size of Pt are favored the C−O bond cleavage reactions, in agreement with Lercher and co-workers.[23]

With PtNi/CZA catalyst, the changes in X^L and X^G are very small, so they would indicate the greater stability of this catalyst as compared to Pt/CZA. The EXAFS characterization will have as its main objective to prove the stability of the metallic phases of PtNi/CZA catalyst.

Figure 5 shows k^3-weighted Fourier transforms (FT) of EXAFS signals of Ni/CZA, Pt/CZA, and PtNi/CZA fresh samples at the Ni K and Pt L_3 edges as compared to that of the corresponding metallic foil. From the results at the Ni K-edge,

Table 1. Results of APR of GLY[a]

					% on a dry basis						
catalysts	T (°C)	X^T	X^G	X^L	SH_2	SCO_2	SCH_4	S_LC_1	S_LC_2	S_LC_3	carbon balance (%)
Ni/CZA	250	17	4	13	50	28.4	5.0	2.2	12.7	50.2	98.5
Pt/CZA	250	60	29	31	77	45.0	2.6	1.6	14.9	33.2	97.3
PtNi/CZA	250	100	39	61	63	35.2	9.4	2.2	31.8	18.2	96.8
Pt/CZA	200	9	4	5	72	41.5	3.4	1.5	12.0	40.0	98.8
PtNi/CZA	200	15	3	12	43	19.0	1.0	0.0	11.2	68.2	99.8

[a]Reaction conditions: 10 wt % glycerol, P = 44 bar, mass of catalysts = 0.5 g, reaction time = 2 h.

dx.doi.org/10.1021/jp412512x | J. Phys. Chem. C 2014, 118, 23645−23653

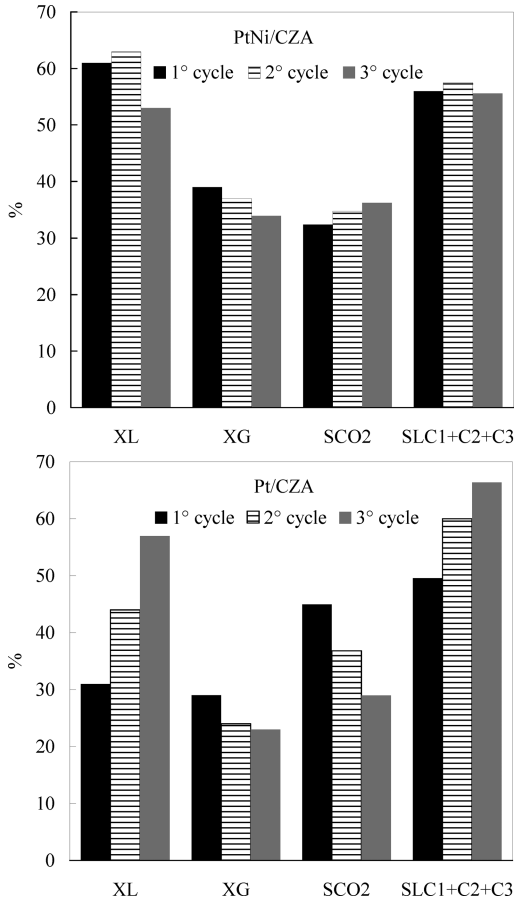

Figure 4. Conversion to gas (X^G), conversion to liquid (X^L), selectivity (%) to CO_2, and $S_L(C_1+C_2+C_3)$ as a function of cycles of reaction for PtNi/CZA and Pt/CZA after 2 h of reaction.

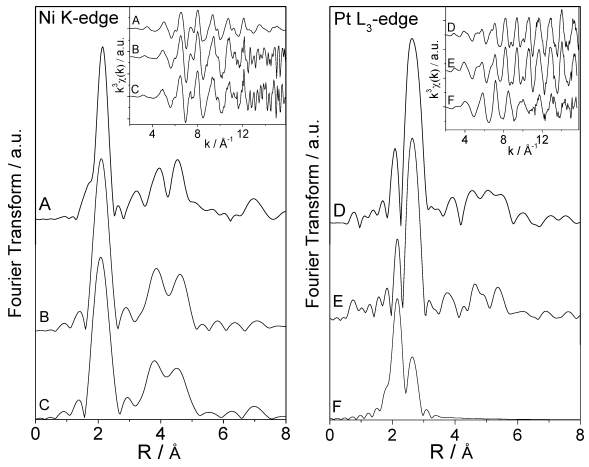

Figure 5. k^3-weighted Fourier transform and the extracted EXAFS signals of the monometallic Ni/CZA(B) and Pt/CZA(E) and bimetallic PtNi/CZA (C and F) catalysts and their corresponding metallic foils (A and D).

it can be seen that all three FT of the EXAFS spectra (A, B, and C) are very similar. The same similarities can be observed when the Pt/CZA (E) is compared to the Pt foil (D) at the Pt L_3-edge. This indicates that both Ni and Pt atoms are in metallic state forming small particles in these catalysts. In contrast, the bimetallic catalyst PtNi/CZA (F) shows a different Fourier transform at the Pt L_3-edge with two peaks at 2.2 and 2.6 Å approximately (without phase corrections), indicating that Pt atoms are immersed in a more complex structure than in the monometallic catalyst. To quantitatively analyze these data, the main peaks were isolated and fitted using standard procedures. The resulting fits and the structural parameters obtained are shown in Figure 6 and Table 2. The EXAFS spectra at the Ni

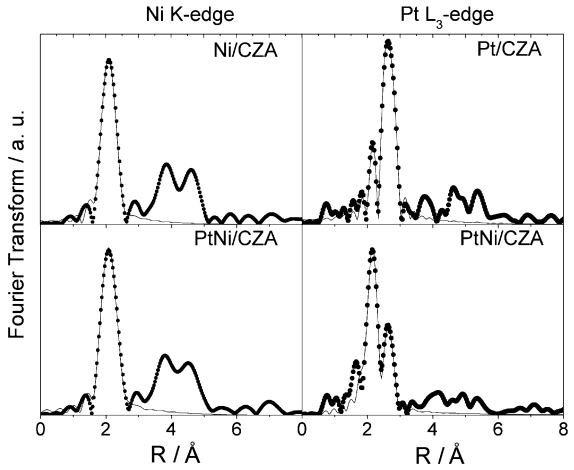

Figure 6. EXAFS fits of fresh catalysts in *R*-space at both edges (●, experimental data; –, fits).

K-edge of both Ni/CZA and PtNi/CZA fresh catalyst were fitted using only a Ni–Ni shell. In both catalysts, a decrease of the average coordination number Ni–Ni ($N_{Ni-Ni} \approx 7 \pm 1$) from that of bulk Ni (12) was found. This could be explained in terms of the size of the cluster, if the Ni clusters were in the range of a few nanometers. Because of the fact that the TEM and DRX results indicate that the Ni particles are higher than 16 nm, this coordination number $N_{Ni-Ni} \approx 7 \pm 1$ would be indicating that the shape of the Ni particle is not spherical but that it would adopt a flat structure.

The Pt/CZA sample was fitted with only one Pt–Pt shell. The existence of only Pt atoms in the vicinity of the absorber is indicating that the Pt is in metallic form. However, the average coordination number of the Pt–Pt shell is 7.2 ± 0.4, smaller than the value of 12, which is the coordination number for the Pt in bulk Pt. In this case, and considering TEM results, we can understand the low value in the average coordination number obtained from the fits, in terms of the size of the Pt particles. This decrease with respect to the bulk metal indicates the formation of very small Pt metallic particles dispersed over the support. Assuming hemispherical particles, estimates of the particle average size can be made[25] from a correlation with the average coordination number N_{Pt-Pt}, and it results in a size of 2 nm in agreement with TEM results.

The FT of the EXAFS signal at the Pt L_3-edge corresponding to the PtNi/CZA fresh sample was fitted in the region between 1.5 and 3 Å using two coordination shells around Pt (one formed by nickel atoms and the other one formed by platinum atoms).

Results of the fits are shown in Table 2 and Figure 6. Both shells have similar coordination numbers (N_{Pt-Ni} 3.4 ± 0.6 and N_{Pt-Pt} 3.8 ± 0.9) totaling the same number of first neighbors as in Pt/CZA catalyst (N_{Pt-Pt} 7.2 ± 0.4). This shows that Pt is again well dispersed in the bimetallic catalyst. The presence of the Pt–Ni shell is an indication of the interaction between the two metals resulting in the formation of Ni–Pt alloy in the

dx.doi.org/10.1021/jp412512x | J. Phys. Chem. C 2014, 118, 23645–23653

Table 2. Results Obtained from the EXAFS Fits of the Different Catalysts[a]

sample	pair	N	R/Å	ΔE/eV	σ^2/Å^2	r-factor
Ni/CZA	Ni−Ni	7.1 ± 1	2.47 ± 0.01	−3.0 ± 0.7	0.004 ± 0.001	0.003
Pt/CZA	Pt−Pt	7.2 ± 0.4	2.76 ± 0.01	1.0 ± 0.3	0.0053 ± 0.0002	0.003
PtNi/CZA fresh	Ni−Ni	7.0 ± 1	2.48 ± 0.01	−4 ± 2	0.004 ± 0.001	0.005
	Pt−Ni	3.4 ± 0.6	2.55 ± 0.01	2 ± 1	0.006 ± 0.001	0.005
	Pt−Pt	3.8 ± 0.9	2.71 ± 0.01	3 ± 1	0.004 ± 0.001	
PtNi/CZA after 1 h of reaction	Ni−Ni	8.6 ± 1.6	2.51 ± 0.01	−4 ± 1	0.008 ± 0.001	0.002
	Pt−Ni	6.5 ± 0.8	2.56 ± 0.01	2 ± 1	0.0069 ± 0.0008	0.002
	Pt−Pt	2.7 ± 0.9	2.71 ± 0.01	3 ± 2	0.004 ± 0.001	
PtNi/CZA after 2 h of reaction	Ni−Ni	9.4 ± 0.9	2.50 ± 0.01	−4 ± 1	0.0076 ± 0.0008	0.001
	Pt−Ni	6.5 ± 0.5	2.56 ± 0.01	3 ± 1	0.0064 ± 0.0004	0.002
	Pt−Pt	2.1 ± 0.5	2.70 ± 0.01	3 ± 2	0.004 ± 0.001	
PtNi/CZA after three reaction cycles	Ni−Ni	8.5 ± 1	2.51 ± 0.01	−4 ± 1	0.008 ± 0.001	0.002
	Pt−Ni	6.4 ± 0.5	2.57 ± 0.01	3 ± 1	0.0070 ± 0.0005	0.002
	Pt−Pt	2.8 ± 0.6	2.71 ± 0.01	3 ± 1	0.0046 ± 0.0006	

[a] N: Average coordination number. R: Interatomic distance. σ^2: Debye−Waller factor.

sample. As the method of preparation of the PtNi/CZA catalyst is adding Pt on the Ni/CZA catalysts, it is expected that the Pt−Ni alloy is formed on the surface of the Ni particles. In addition, as the amount of nickel is higher than platinum (Ni/Pt atomic relation = 16.5), not all of the Ni would be forming alloy, and therefore the majority of Ni atoms will still be forming monometallic flat Ni particles.

The Pt−Pt shell can be due to the alloy or a different metallic phase. With EXAFS being an average technique that probes the local structure around a specific element, the fitted coordination numbers are averaged over all absorbing atoms present in the sample. Because of this, it is difficult to extract direct structural information from the coordination numbers, but some conclusion can be made when comparing the relation of the different coordination numbers and the bond distances with those of the bulk materials.[26] For this purpose, we compared our results with the first shells of different Ni−Pt alloys to estimate the structures formed in PtNi/CZA catalyst. Considering the Ni/Pt atomic relation in the catalyst, we would expect a Ni-rich alloy. However, we must consider that at the nanoscale a great proportion of atoms are on the surface, which makes cluster surface energy terms to be determinant in the dependence of the structure and thermodynamics of the particle.[27,28] Therefore, mixed or disordered alloys are possible so we did not restrict our analysis to Ni-rich alloys. In particular, Pt_3Ni, PtNi, and $PtNi_3$ alloys were chosen[29,30] for the EXAFS analysis. In Pt_3Ni, the Pt−Ni distance is 2.713 Å, which is longer than the value fitted from our results (2.55 Å), with a difference of 0.163 Å.

It is expected that the contraction of the bond distances should be smaller than 0.1 Å, because of the small size of the particles for subnanometer bare supported Pt clusters at room temperature.[31−34] Therefore, a difference of 0.163 Å allows us to discard the presence of Pt_3Ni alloy. The Pt−Ni bond distances in the other two alloys (PtNi and $PtNi_3$) are smaller (2.662 and 2.578 Å, respectively) and longer than the fitted value, but within the expected contraction range. However, the fitted value for the Pt−Ni bond distance (2.55 Å) is very similar to 2.578 Å, indicating that $PtNi_3$ alloy is the most probable in the PtNi/CZA sample.

In PtNi/CZA catalyst, the coordination number N_{Pt-Pt} (3.8 ± 0.9) would indicate that an unalloyed metallic Pt phase would be present. Thus, from our results we can conclude that Pt atoms are present in two different phases: a $PtNi_3$ alloy on the surface of the Ni particles and unalloyed metallic Pt. The fitted coordination numbers then would be an average over the N_{Pt-Ni} and N_{Pt-Pt} on both phases, weighted by the proportion of each phase in the sample.[35] As the average coordination numbers N_{Pt-Pt} (3.8 ± 0.9) and N_{Pt-Ni} (3.4 ± 0.6) are very similar and assuming that particle size is similar for unalloyed Pt and alloyed Pt, we can conclude that the proportion of each phase is approximately 50%.

The absence of a Ni−Pt shell in the EXAFS results at the Ni K-edge may seem to contradict the existence of the alloy, but it can be understood when taking into account the ratio of Ni and Pt atoms in the catalyst, resulting in an averaged coordination number Ni−Pt too small to be determined form the EXAFS analysis.

When analyzing the results of the EXAFS fits of the used samples (after 1 h, 2 h, and three reaction cycles) (Table 2), some small changes in the average coordination numbers are observed when comparing these results with those obtained for the PtNi/CZA fresh catalyst. From the Ni K-edge results, an increase of the Ni−Ni coordination number is found. From the Pt L_3-edge, the total coordination number for Pt (N_{Pt-Ni} + N_{Pt-Pt}) is greater than that of the fresh catalyst. In particular, an increase of the N_{Pt-Ni} and a decrease of the N_{Pt-Pt} is observed; these results show that there is a growth of the alloy phase at the expense of the segregated metallic Pt phase.

Despite the variations observed in the coordination numbers of used samples, the Pt−Pt and Pt−Ni bond distances stay unchanged in comparison with the fresh samples. This way, when comparing the fresh catalyst and all used catalysts (1 h, 2 h, and three reaction cycles), we can conclude that the reaction medium favored the formation of the alloy $PtNi_3$.

For the used samples, the average coordination number N_{Pt-Pt} is 2.7 ± 0.9 and N_{Pt-Ni} is 6.5 ± 0.8, and assuming that particle size is similar for unalloyed Pt and alloyed Pt, we can conclude that 70% of Pt atoms, approximately, would be forming the alloy, while the other 30% would be forming unalloyed nanoparticles.

In Table 3 are shown the results obtained by XPS for the catalyst PtNi/CZA fresh and after 1 h of reaction, where the binding energy (BE) of the Pt $4f_{7/2}$, Ni $2p_{3/2}$, Ce $3d_{5/2}$, Zr $3d_{5/2}$, and Al 2p is shown. The occurrence of a strong interaction between ceria and zirconia is evidenced by the decrease in the BE of Zr $3d_{5/2}$ (181.6−181.8 eV) with respect to the value for ZrO_2 (182.5 eV), as reported in the bibliography.[36] The Ce 3d

dx.doi.org/10.1021/jp412512x | J. Phys. Chem. C 2014, 118, 23645−23653

Table 3. Characterization by XPS: Binding Energies (eV) and Surface Atomic Ratios for PtNi/CZA Catalysts

catalyst	PtNi/CZA fresh	PtNi/CZA after 1 h of reaction[a]
Pt $4f_{7/2}$ (eV)	70.9	70.9
Ni $2p_{3/2}$ (eV)	851.78 (Ni^0, 73%)	851.79 (Ni^0, 75%)
	855.3 (Ni^{2+}, 27%)	855.2 (Ni^{2+}, 25%)
Ce $3d_{5/2}$ (eV)	881.2 (v)	881.1 (v)
	885.0 (v′)	885.3 (v′)
	916.2 (u‴, 2%)	916.6 (u‴, 3%)
Zr $3d_{5/2}$ (eV)	181.7	181.6
Al 2p (eV)	73.9	73.9
Ni/Pt (bulk)	0.436 (16.6)	0.889
Ni/(Al+Ce+Zr) (bulk)	0.0089 (0.045)	0.0095
Pt/(Al+Ce+Zr) (bulk)	0.0204 (0.0027)	0.0107

[a]After the reaction was dried, calcined, and reduced in flowing H_2/Ar mixture in situ.

region shows the presence of both Ce^{4+} and Ce^{3+} oxidation states. Because the u‴ peak arises exclusively from Ce^{4+}, it can be used as a quantitative measure of Ce^{4+} amount. The integrated area of the u‴ component with respect to the total Ce 3d area should constitute around 14% of the total integral intensity.[37]

For the PtNi/CZA catalyst in the region corresponding to Pt $4f_{7/2}$ at 70.9 eV, there appears one peak indicating the complete reduction of platinum. The Ni $2p_{3/2}$ spectra consisted of both Ni^0 and Ni^{2+}, suggesting that the applied reduction procedure (at 400 °C in H_2 5%/Ar flux in the pretreatment chamber of the XPS equipment) did not result in a complete reduction of the nickel. XPS results of surface atomic ratios show a decrease of Pt atoms on the surface from 0.0204 to 0.0107. TEM results of PtNi/CZA used sample are included in the Supporting Information. It was observed in the PtNi/CZA used sample, after 1 h of reaction, a decrease in the quantity of Pt particles smaller than 2 nm, which agrees with the XPS results. This could be due to the diffusion of Pt atoms to the core of Ni particles, or to the mobility of Ni atoms in the reaction conditions, which can cover Pt atoms that were initially located on their surface. Both explanations are compatible with the observed increase of the N_{Pt-Ni} coordination numbers in all used samples.

Figure 7 shows k^3-weighted Fourier transforms of EXAFS signals of the bimetallic catalysts PtNi/CZA at the Ni K-edge and at the Pt L_3-edge after 1 and 2 h of use in the reaction and after three complete cycles. If we compare the catalyst used for 1 h with the one used for 2 h and the one after three reaction cycles, it can be observed that all average coordination numbers remain almost unchanged, which shows that the phase changes occur mainly in the first hour of use (Figure 8). This result would explain the moderate modification of the activity and selectivity of PtNi/CZA (Figure 4).

The EXAFS results confirm that the higher stability of the PtNi/CZA catalyst in the APR of glycerol is due to the presence of the alloy on the surface of the Ni particles that stabilizes the catalyst. The changes in their structure are small and take place during the first minutes of reaction, reaching at that point a stable state.

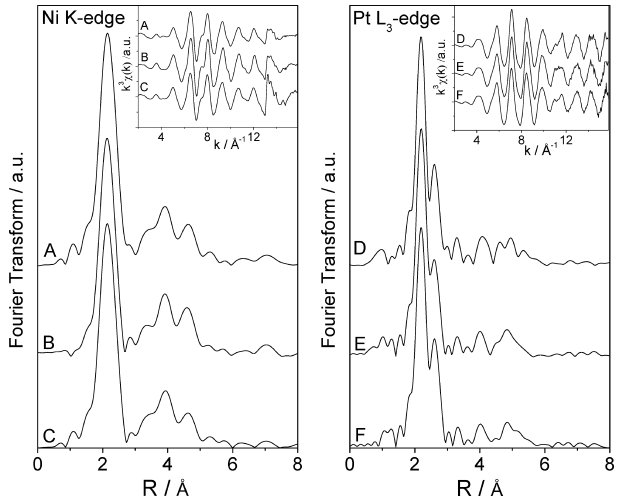

Figure 7. k^3-weighted Fourier transform and the extracted EXAFS signals of the bimetallic PtNi/CZA catalysts after 1 h of use (A and D) and 2 h of use (B and E) and after three complete cycles (C and F).

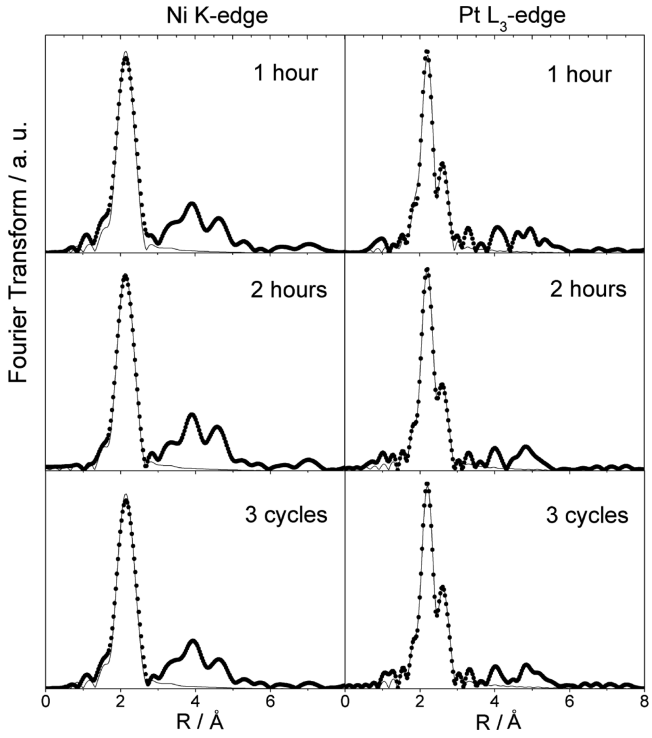

Figure 8. EXAFS fits of used catalysts after 1 and 2 h of reaction and after three reaction cycles in *R*-space at both edges (●, experimental data; −, fits).

4. CONCLUSIONS

In this work, the Pt and Ni catalysts supported on α-Al_2O_3 modified with CeO_2 and ZrO_2 in the glycerol liquid-phase conversion were studied, and EXAFS characterizations were carried out with the aim of determining the structure of the metallic phases.

The Ni/CZA catalyst presents very low activity, whereas the Pt/CZA catalyst presents higher selectivity to the glycerol reforming (SCO_2 = 45%), but it is not stable.

The bimetallic catalyst PtNi/CZA presents the highest activity and promotes the formation of liquid oxygenated

dx.doi.org/10.1021/jp412512x | J. Phys. Chem. C 2014, 118, 23645−23653

hydrocarbons, mainly acetol and 1,2-propylene glycol, which are formed from glycerol hydrogenolysis.

It was determined by EXAFS analyses that in the bimetallic catalyst PtNi/CZA, three phases would be present: the Ni would form mostly metallic nanoparticles, at least 50% of the Pt atoms would form $PtNi_3$ alloy nanoparticles on the surface of the bigger Ni particles, and the rest of the Pt atoms remain unalloyed with high dispersion forming small nanoparticles.

Taking into account the catalytic results, in the PtNi/CZA catalyst the highest activity could be assigned to the presence of the $PtNi_3$ alloy that results in a more active phase than the Pt and Ni sites separately. The higher stability of the PtNi/CZA catalyst would be associated with the presence of the $PtNi_3$ alloy nanoparticles on the surface of the Ni particles with low mobility. The catalyst reaches a stable state during the first hour of reaction, and a small increase in the particles size is observed as well as an increase in the quantity of alloy. These metallic phases remain then unalterable after three complete cycles of reaction with stable levels of conversion and selectivity.

■ ASSOCIATED CONTENT

Supporting Information

TEM results, XPS results, EXAFS results, and turnover frequency TOF values. This material is available free of charge via the Internet at http://pubs.acs.org.

■ AUTHOR INFORMATION

Corresponding Author

*E-mail: nnichio@quimica.unlp.edu.ar.

Notes

The authors declare no competing financial interest.

■ ACKNOWLEDGMENTS

We are thankful for the financial support received from ANPCyT (Argentina, PICT no. 1962, PICT no. 2008-00038, and Proyect PRH 200-7), UNLP (Argentina, Proyect I-175), CONICET (Argentina, PIP no. 542 and PIP no. 3079), and LNLS (Brasil, Proyect XAFS1-15239).

■ REFERENCES

(1) Cortright, R. D.; Davda, R. R.; Dumesic, J. A. Hydrogen from Catalytic Reforming of Biomass-Derived Hydrocarbons in Liquid Water. *Nature* **2002**, *418*, 964−967.

(2) Davda, R. R.; Shabaker, J. W.; Huber, G. W.; Cortright, R. D.; Dumesic, J. A. Aqueous-Phase Reforming of Ethylene Glycol on Silica-Supported Metal Catalysts. *Appl. Catal., B* **2003**, *43*, 13−26.

(3) Shabaker, J. W.; Huber, G. W.; Davda, R. R.; Cortright, R. D.; Dumesic, J. A. Aqueous-Phase Reforming of Ethylene Glycol over Supported Platinum Catalysts. *Catal. Lett.* **2003**, *88*, 1−8.

(4) Soares, R. R.; Simonetti, D. A.; Dumesic, J. A. Glycerol as a Source for Fuels and Chemicals by Low-Temperature Catalytic Processing. *Angew. Chem., Int. Ed.* **2006**, *45*, 3982−3985.

(5) Huber, G. W.; Shabaker, J. W.; Evans, S. T.; Dumesic, J. A. Aqueous-Phase Reforming of Ethylene Glycol over Supported Pt and Pd Bimetallic Catalysts. *Appl. Catal., B* **2006**, *62*, 226−235.

(6) Gürbüz, E. I.; Kunkes, E. L.; Dumesic, J. A. Integration of C−C Coupling Reactions of Biomass-Derived Oxygenates to Fuel-Grade Compounds. *Appl. Catal., B* **2010**, *94*, 134−141.

(7) Valenzuela, M. B.; Jones, C. W.; Agrawal, P. K. Batch Aqueous-Phase Reforming of Woody Biomass. *Energy Fuels* **2006**, *20*, 1744−1752.

(8) Wen, G.; Xu, Y.; Ma, H.; Xu, Z.; Tian, Z. Production of Hydrogen by Aqueous-Phase Reforming of Glycerol. *Int. J. Hydrogen Energy* **2008**, *33*, 6657−6666.

(9) Manfro, R. L.; da Costa, A. F.; Ribeiro, N. F. P.; Souza, M. M. Hydrogen Production by Aqueous-Phase Reforming of Glycerol over Nickel Catalysts Supported on CeO_2. *Fuel Process. Technol.* **2011**, *92*, 330−335.

(10) Menezes, A. O.; Rodrigues, M. T.; Zimmaro, A.; Borges, L. E. P.; Fraga, M. A. Production of Renewable Hydrogen from Aqueous-Phase Reforming of Glycerol over Pt Catalysts Supported on Different Oxides. *Renewable Energy* **2011**, *36*, 595−599.

(11) Huber, G. W.; Shabaker, J. W.; Dumesic, J. A. Raney Ni-Sn Catalyst for H_2 Production from Biomass-Derived Hydrocarbons. *Science* **2003**, *300*, 2075−2077.

(12) Shabaker, J. W.; Huber, G. W.; Dumesic, J. A. Aqueous-Phase Reforming of Oxygenated Hydrocarbons over Sn-modified Ni Catalysts. *J. Catal.* **2004**, *222*, 180−191.

(13) King, D.; Zhang, L.; Xia, G.; Karim, A.; Heldebrant, D.; Wang, X.; Peterson, T.; Wang, Y. Aqueous Phase Reforming of Glycerol for Hydrogen Production over Pt−Re Supported on Carbon. *Appl. Catal., B* **2010**, *99*, 206−213.

(14) Zhang, L.; Karim, A. M.; Engelhard, M. H.; Wei, Z.; King, D. L.; Wang, Y. Correlation of Pt−Re Surface Properties with Reaction Pathways for the Aqueous-Phase Reforming of Glycerol. *J. Catal.* **2012**, *287*, 37−43.

(15) Iriondo, A.; Cambra, J. F.; Barrio, V. L.; Guemez, M. B.; Arias, P. L.; Sanchez-Sanchez, M. C.; Navarro, R. M.; Fierro, J. L. Glycerol Liquid Phase Conversion over Monometallic and Bimetallic Catalysts: Effect of Metal, Support Type and Reaction Temperatures. *Appl. Catal., B* **2011**, *106*, 83−93.

(16) Doukkali, M. E.; Iriondo, A.; Arias, P. L.; Requies, J.; Gandarías, I.; Jalowiecki-Duhamel, L.; Dumeignil, F. A comparison of Sol−Gel and Impregnated Pt or/and Ni Based γ-Alumina Catalysts for Bioglycerol Aqueous Phase Reforming. *Appl. Catal., B* **2012**, *125*, 516−529.

(17) Ravenelle, R.; Copeland, J.; Kim, W.; Crittenden, J.; Sievers, C. Structural Changes of γ-Al_2O_3-Supported Catalysts in Hot Liquid Water. *ACS Catal.* **2011**, *1*, 552−561.

(18) Pompeo, F.; Gazzoli, D.; Nichio, N. N. Characterization of α-Al_2O_3 Supports Modified with CeO_2 and ZrO_2. *Mater. Lett.* **2009**, *63*, 477−479.

(19) Ravel, B.; Newville, M. ATHENA, ARTEMIS, HEPHAESTUS: Data Analysis for X-ray Absorption Spectroscopy using IFEFFIT. *J. Synchrotron Radiat.* **2005**, *12*, 537−541.

(20) Zabinsky, S. I.; Rehr, J. J.; Ankudinov, A.; Albers, R. C.; Eller, M. J. Multiple-Scattering Calculations of x-Ray-Absorption Spectra. *Phys. Rev. B* **1995**, *52*, 2995−3009.

(21) Abu Bakar, N. H. H.; Bettahar, M. M.; Abu Bakar, M.; Monteverdi, S.; Ismail, J.; Alnot, M. PtNi Catalysts Prepared Via Borohydride Reduction for Hydrogenation of Benzene. *J. Catal.* **2009**, *265*, 63−71.

(22) Pompeo, F.; Nichio, N. N.; Souza, M. M.; Cesar, D. V.; Ferretti, O. A.; Schmal, M. Study of Ni and Pt Catalysts Supported on α-Al_2O_3 and ZrO_2 Applied in Methane Reforming with CO_2. *Appl. Catal., A* **2007**, *316*, 175−183.

(23) Wawrzetz, A.; Peng, B.; Hrabar, A.; Jentys, A.; Lemonidou, A. A.; Lercher, J. A. Towards Understanding the Bifunctional Hydrodeoxygenation and Aqueous Phase Reforming of Glycerol. *J. Catal.* **2010**, *269*, 411−420.

(24) Barbelli, M. L.; Pompeo, F.; Santori, G. F.; Nichio, N. N. Pt Catalyst Supported on α-Al_2O_3 Modified with CeO_2 and ZrO_2 for Aqueous-Phase-Reforming of Glycerol. *Catal. Today* **2013**, *213*, 58−64.

(25) Frenkel, A. I.; Hills, C. W.; Nuzzo, R. G. A View from the Inside: Complexity in the Atomic Scale Ordering of Supported Metal Nanoparticles. *J. Phys. Chem. B* **2001**, *105*, 12689−12703.

(26) Frenkel, A. I.; Yevick, A.; Cooper, C.; Vasic, R. Modeling the Structure and Composition of Nanoparticles by Extended X-Ray Absorption Fine-Structure Spectroscopy. *Annu. Rev. Anal. Chem.* **2011**, *4*, 23−39.

(27) Schmidt, M.; Kusche, R.; Hippler, T.; Donges, J.; Kronmüller, W.; von Issendorff, B.; Haberland, H. Negative Heat Capacity for a Cluster of 147 Sodium Atoms. *Phys. Rev. Lett.* **2001**, *86*, 1191−1195.
(28) Giovanetti, L. J.; Ramallo-López, J. M.; Requejo, F. G.; Garcia-Gutierrez, D. I.; Jose-Yacaman, M.; Craievich, A. F. Anomalous Vibrational Properties Induced by Surface Effects in Capped Pt Nanoparticles. *J. Phys. Chem. C* **2007**, *111*, 7599−7604.
(29) Leroux, C.; Cadeville, M. C.; Pierron-Bohnes, V.; Inden, G.; Hinz, F. Comparative Investigation of Structural and Transport Properties of L10 NiPt and CoPt phases; the Role of Magnetism. *J. Phys. F: Met. Phys.* **1988**, *18*, 2033−2051.
(30) Okamoto, H. Ni-Pt (Nickel-Platinum). *J. Phase Equilib. Diffus.* **2010**, *31*, 322.
(31) Wijnen, P. W. J. G.; Van Zon, F. B. M.; Koningsberger, D. C. Determination of Metal Particle Size in Partly Reduced Ni Catalysts by Hydrogen/Oxygen Chemisorption and EXAFS. *J. Catal.* **1988**, *114*, 463−468.
(32) Kang, J. H.; Menard, L. D.; Nuzzo, R. G.; Frenkel, A. I. Unusual Non-Bulk Properties in Nanoscale Materials: Thermal Metal−Metal Bond Contraction of γ-Alumina-Supported Pt Catalysts. *J. Am. Chem. Soc.* **2006**, *128*, 12068−12069.
(33) Bus, E.; Miller, J. T.; Kropf, A. J.; Prins, R.; van Bokhoven, J. A. Analysis of In Situ EXAFS Data of Supported Metal Catalysts Using the Third and Fourth Cumulant. *Phys. Chem. Chem. Phys.* **2006**, *8*, 3248−3258.
(34) Lei, Y.; Jelic, J.; Nitsche, L.; Meyer, R.; Miller, J. Effect of Particle Size and Adsorbates on the L3, L2 and L1 X-ray Absorption Near Edge Structure of Supported Pt Nanoparticles. *Top. Catal.* **2011**, *54*, 334−348.
(35) Frenkel, A. Z. Solving the 3D Structure of Metal Nanoparticles. *Kristallografiya* **2007**, *222*, 605−611.
(36) Nelson, A.; Schulz, K. Surface Chemistry and Microstructural Analysis of $Ce_xZr_{1-x}O_{2-y}$ Model Catalyst Surfaces. *Appl. Surf. Sci.* **2003**, *210*, 206−221.
(37) Shyu, J.; Otto, K.; Watkins, W.; Graham, G.; Belitz, R.; Gandhi, H. Characterization of Pd/γ-Alumina Catalysts Containing Ceria. *J. Catal.* **1988**, *114*, 23−33.